Supplement of

The coupled Southern Ocean–Sea ice–Ice shelf Model (SOSIM v1.0): configuration and evaluation

Chengyan Liu[1*], Zhaomin Wang[1*], Dake Chen[1], Xianxian Han[1], Hengling Leng[1], Xi Liang[2], Liangjun Yan[3], Xiang Li[1], Craig Stevens[4], Andrew McC. Hogg[5], Kazuya Kusahara[6], Kaihe Yamazaki[7], Kay I. Ohshima[8], Meng Zhou[9], Xiao Cheng[10], Dongxiao Wang[3], Changming Dong[11], Jiping Liu[12], Qinghua Yang[12], Xichen Li[13], Ruibo Lei[14], Minghu Ding[15], Zhaoru Zhang[9], Dujuan Kang[9], Di Qi[16], Tongya Liu[17], Jihai Dong[11], Lu An[18], Ru Chen[19], Tong Zhang[20], Xiaoming Hu[12], Bo Han[12], Haibo Bi[21], Qi Shu[22], Longjiang Mu[23], Shiming Xu[24], Hu Yang[1], Hailong Liu[25], Tingfeng Dou[26], Zhixuan Feng[27], Lei Zheng[10], Xueyuan Tang[15], Guitao Shi[28], Yongqing Cai[15], Bingrui Li[15], Yang Wu[29], Xia Lin[11], Wenjin Sun[11], Yu Liu[30], Kai Yu[31], Yu Zhang[32], Weizeng Shao[32], Xiaoyu Wang[33], Shaojun Zheng[34], Chengyi Yuan[35], Chunxia Zhou[36], Jian Liu[1], Yang Liu[12], Yue Xia[12], Xiaoyu Pan[12], Jiabao Zeng[12], Kechen Liu[37], Jiahao Fan[12], Chen Cheng[1], and Qi Li[1]

[1]Southern Marine Science and Engineering Guangdong Laboratory (Zhuhai), Zhuhai, 519080, China
[2]Key Laboratory of Marine Hazards Forecasting, National Marine Environmental Forecasting Center, Ministry of Natural Resources, Beijing, 100081, China
[3]School of Marine Science, Sun Yat-sen University, Zhuhai, 519082, China
[4]Earth Sciences New Zealand, Wellington, 6021, New Zealand
[5]Research School of Earth Sciences and ARC Centre of Excellence for Climate System Science, Australian National University, Canberra, ACT 2600, Australia
[6]Japan Agency for Marine-Earth Science and Technology, Yokohama, 237-0061, Japan
[7]Institute of Marine and Antarctic Studies, University of Tasmania, Hobart, TAS 7001, Australia
[8]Institute of Low Temperature Science, Hokkaido University, Sapporo, 060-0819, Japan
[9]Key Laboratory of Polar Ecosystem and Climate Change, Ministry of Education and School of Oceanography, Shanghai Jiao Tong University, Shanghai, 200240, China
[10]School of Geospatial Engineering and Science, Sun Yat-sen University, 519082, Zhuhai, China
[11]School of Marine Sciences, Nanjing University of Information Science and Technology, Nanjing, 210044, China
[12]School of Atmospheric Sciences, Sun Yat-sen University, Zhuhai, 519082, China
[13]Institute of Atmospheric Physics, Chinese Academy of Sciences, Beijing, 100029, China
[14]Polar Research Institute of China, Shanghai, 200136, China
[15]State Key Laboratory of Severe Weather, Chinese Academy of Meteorological Sciences, Beijing, 100081, China
[16]Polar and Marine Research Institute, Jimei University, Xiamen, 361021, China
[17]State Key Laboratory of Satellite Ocean Environment Dynamics, Second Institute of Oceanography, Ministry of Natural Resources, Hangzhou, 310012, China
[18]College of Surveying and Geo-Informatics, Tongji University, Shanghai, 200092, China
[19]School of Marine Science and Technology, Tianjin University, Tianjin, 300072, China
[20]State Key Laboratory of Earth Surface Processes and Disaster Risk Reduction, Faculty of Geographical Science, Beijing Normal University, Beijing 100875, China
[21]Key Laboratory of Marine Geology and Environment, Institute of Oceanology, Chinese Academy of Sciences, Qingdao, 266071, China
[22]First Institute of Oceanography, and Key Laboratory of Marine Science and Numerical Modeling, Ministry of Natural Resources, Qingdao, 266061, China
[23]Laoshan Laboratory, Qingdao, 266100, China.

[24]Ministry of Education Key Laboratory for Earth System Modeling, Department of Earth System Science, Tsinghua University, Beijing, 100084, China
[25]Yunnan Key Laboratory of Meteorological Disasters and Climate Resources in the Greater Mekong Subregion, Yunnan University, Kunming, 650500, China
[26]College of Resources and Environment, University of Chinese Academy of Sciences, Beijing, 100049, China
[27]State Key Laboratory of Estuarine and Coastal Research, East China Normal University, Shanghai, 200241, China
[28]School of Geographic Sciences and State Key Laboratory of Estuarine and Coastal Research, East China Normal University, Shanghai, 200241, China
[29]School of Information Engineering, Nanjing Xiaozhuang University, Nanjing, 211171, China
[30]Marine Science and Technology College, Zhejiang Ocean University, Zhoushan, 316000, China
[31]Key Laboratory of Marine Hazards Forecasting, Ministry of Natural Resources, Hohai University, Nanjing, 210098, China
[32]College of Oceanography and Ecological Science, Shanghai Ocean University, Shanghai, 201306, China
[33]Frontier Science Center for Deep Ocean Multispheres and Earth System, Ocean University of China, Qingdao, 266100, China
[34]Key Laboratory of Climate, Resources and Environment in Continental Shelf Sea and Deep Sea of Department of Education of Guangdong Province, Guangdong Ocean University, Zhanjiang, 524088, China
[35]Department of Marine Technology, College of Marine and Environmental Sciences, Tianjin University of Science and Technology, Tianjin, 300457, China
[36]Chinese Antarctic Centre of Surveying and Mapping, Wuhan University, Wuhan, 430079, China
[37]College of Meteorology and Oceanography, National University of Defense Technology, Changsha, 410073, China

Correspondence to: Chengyan Liu (liuchengyan@sml-zhuhai.cn); Zhaomin Wang (wangzhaomin@sml-zhuhai.cn)

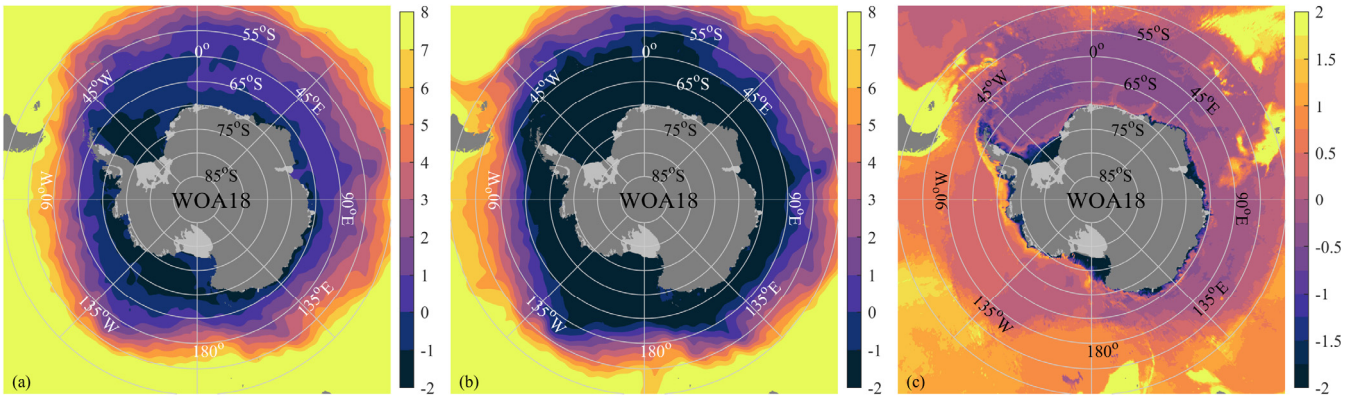

Fig. S1. The horizontal distribution of θ (°C). **(a)** Climatological SST in summer from WOA18. **(b)** As in **(a)**, but for SST in winter. **(c)** As in **(a)**, but for the climatological annual mean θ at the bottom layer.

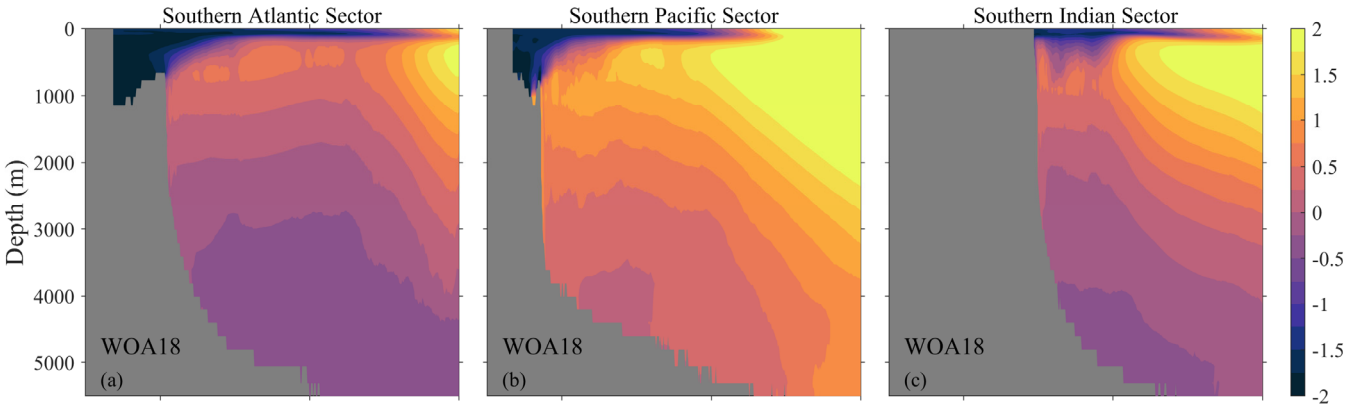

Fig. S2. The vertical distribution of zonally averaged θ (°C). **(a)** Climatological annual mean of zonally averaged θ in the Southern Atlantic sector from WOA18. The zonal average is calculated by omitting dry grids. **(b)** and **(c)** As in **(a)**, but for the Southern Pacific and Southern Indian sectors, respectively.

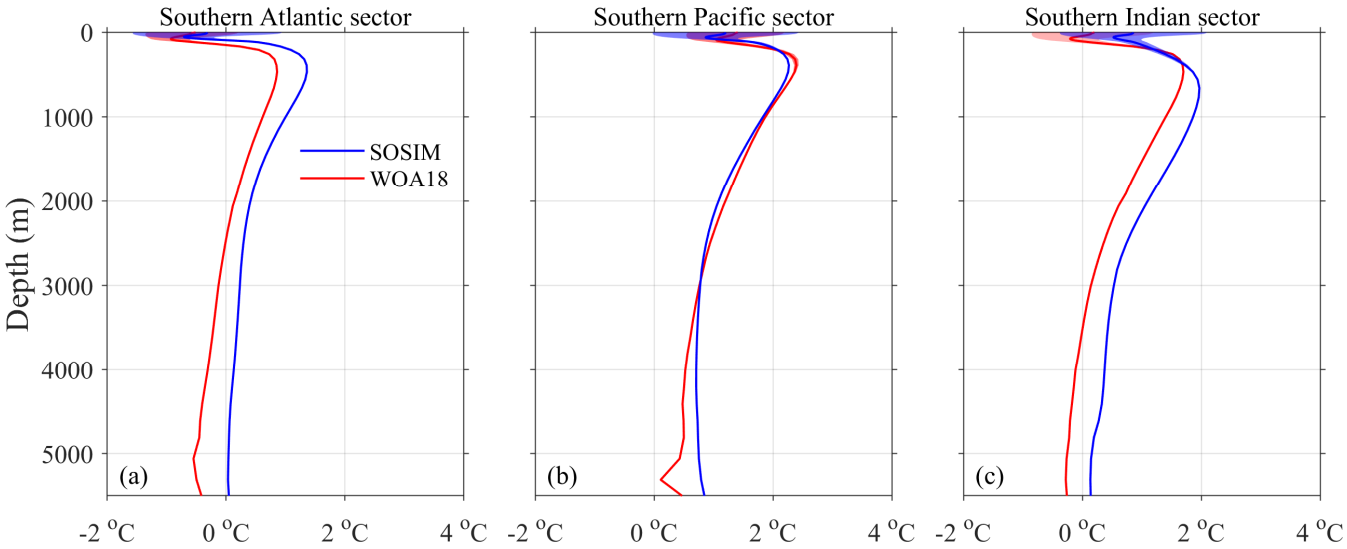

Fig. S3. The vertical profiles of horizontally area-averaged θ (°C). **(a)** The horizontally area-averaged θ within the Southern Atlantic sector (semi-transparent red region in Fig. 5a in the manuscript). Semi-transparent color shading denotes the STD of monthly climatology. **(b)** and **(c)** As in **(a)**, but for the Southern Pacific and Southern Indian sectors, respectively.

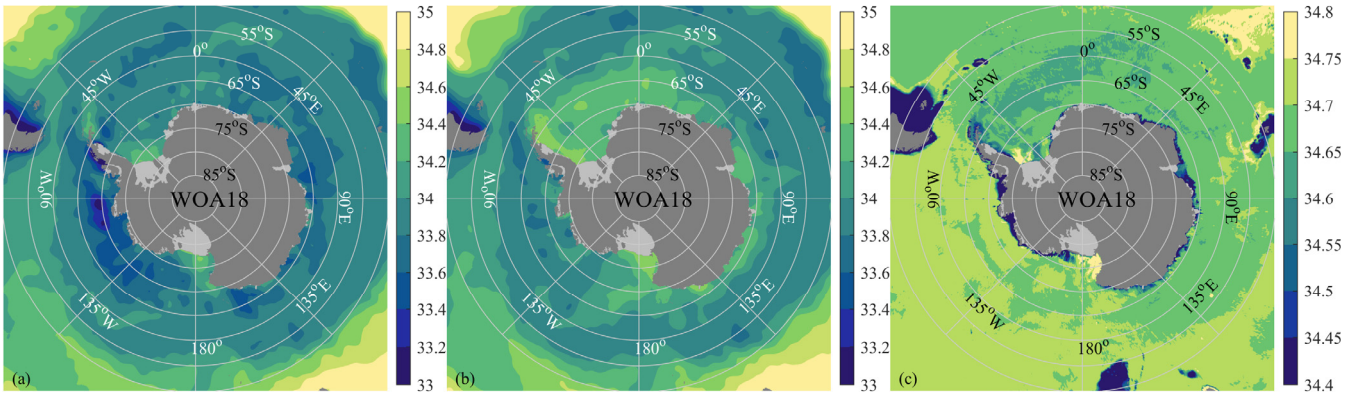

Fig. S4. As in Fig. S1, but for the horizontal distribution of *S* (psu).

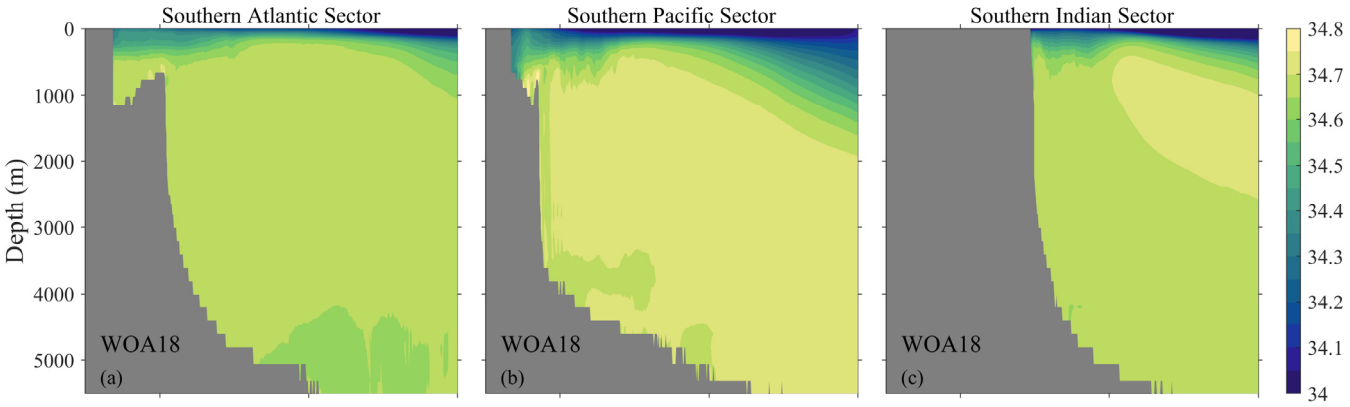

Fig. S5. As in Fig. S2, but for the vertical distribution of zonally averaged *S* (psu).

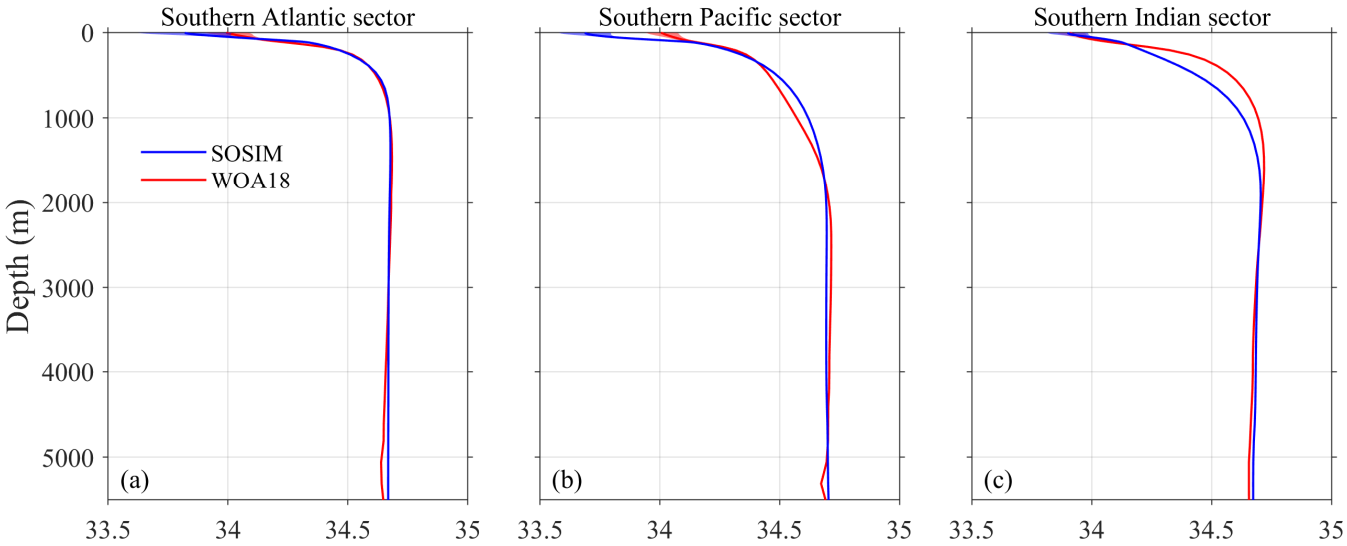

Fig. S6. As in Fig. S3, but for the horizontally area-averaged *S* (psu).

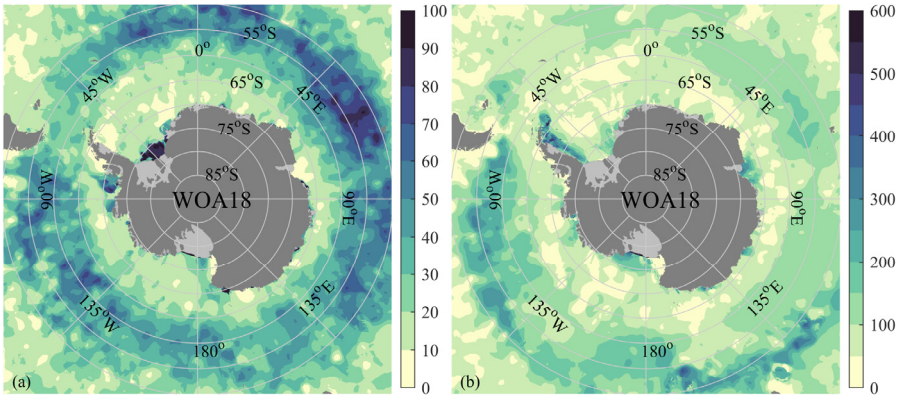

Fig. S7. The horizontal distribution of MLD (m). **(a)** The MLD of WOA18 in the austral summer. **(b)** As in **(a)**, but for the MLD in the austral winter.

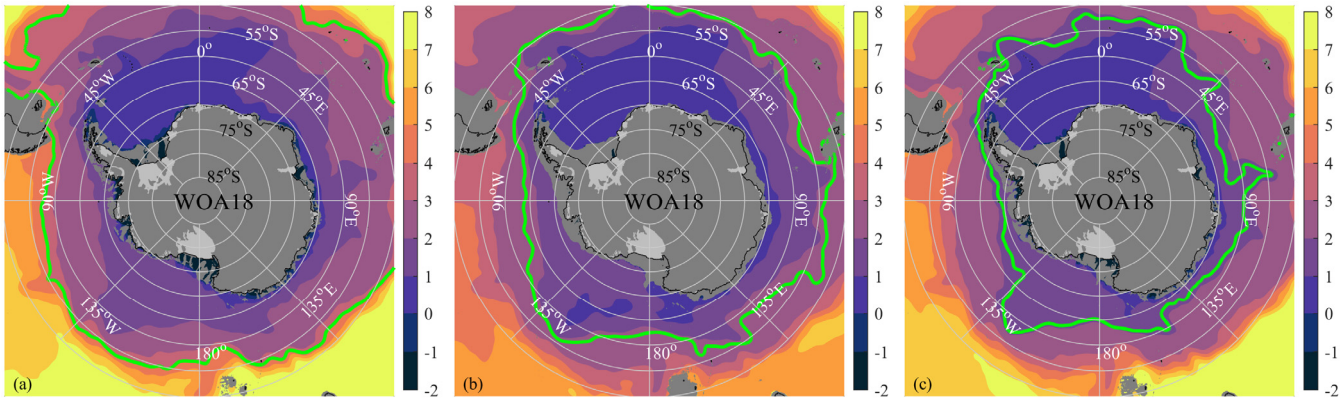

Fig. S8. The circumpolar distribution of the SAF, PF, and SACCF in WOA18, with θ (°C) at corresponding depths in color. **(a)** The SAF (the green line, 4 °C isotherm) and θ (°C) at 400 m depth. **(b)** As in **(a)**, but for the PF (2.2 °C isotherm) and θ (°C) at 800 m depth. **(c)** As in **(a)**, but for the SACCF (1.8 °C isotherm) and θ (°C) at 500 m depth.

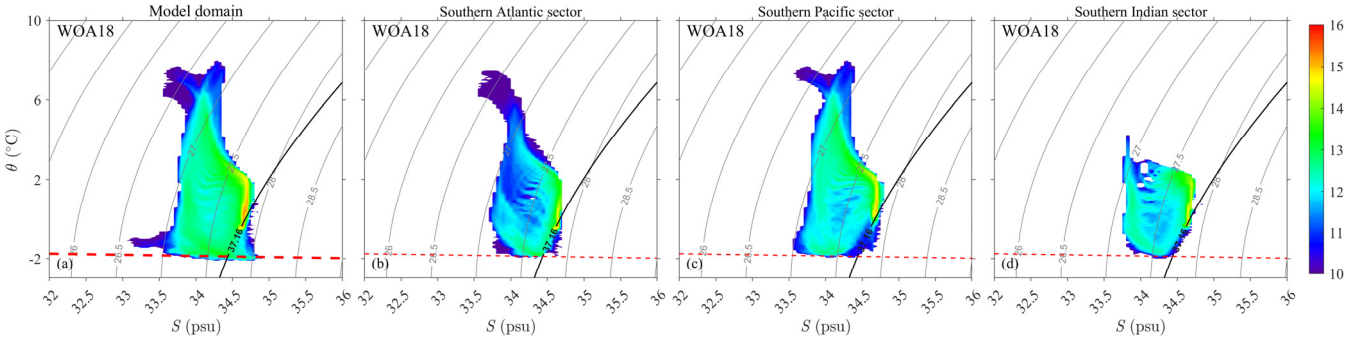

Fig. S9. (a) Climatological water mass volume (log10 (V), m^3) distribution in θ–S space (bins of 0.05 °C by 0.05 psu size) in the inner model domain in WOA18, superimposed with potential density σ_0 (grey lines) in contour intervals of 0.5 kg m^{-3}. The red dashed line denotes the surface freezing point of seawater. The black lines denote the σ_2 contours of 37.16 kg m^{-3}, indicating the threshold between CDW and AABW. **(b-d)** As in **(a)**, but for the Southern Atlantic sector, the Southern Pacific sector, and the Southern Indian sector, respectively.

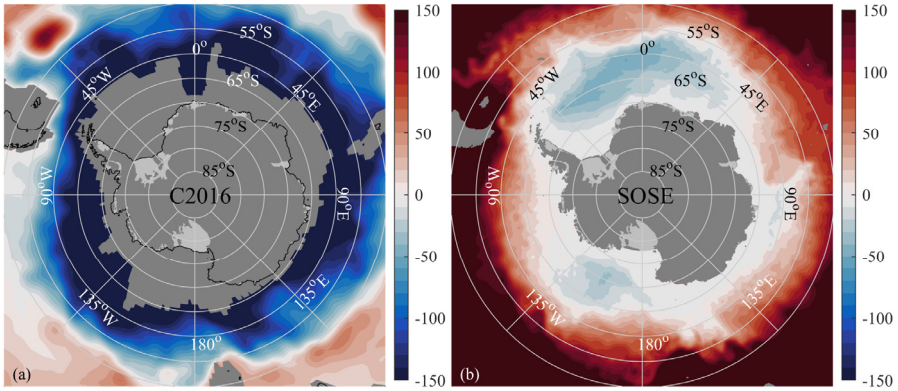

105

Fig. S10. The barotropic stream function. **(a)** The climatological Ψ (Sv) estimated from the C2016. The grey region over the open ocean indicates the absence of observational estimation. **(b)** As in **(a)**, but for SOSE. Negative cells denote cyclonic circulations.

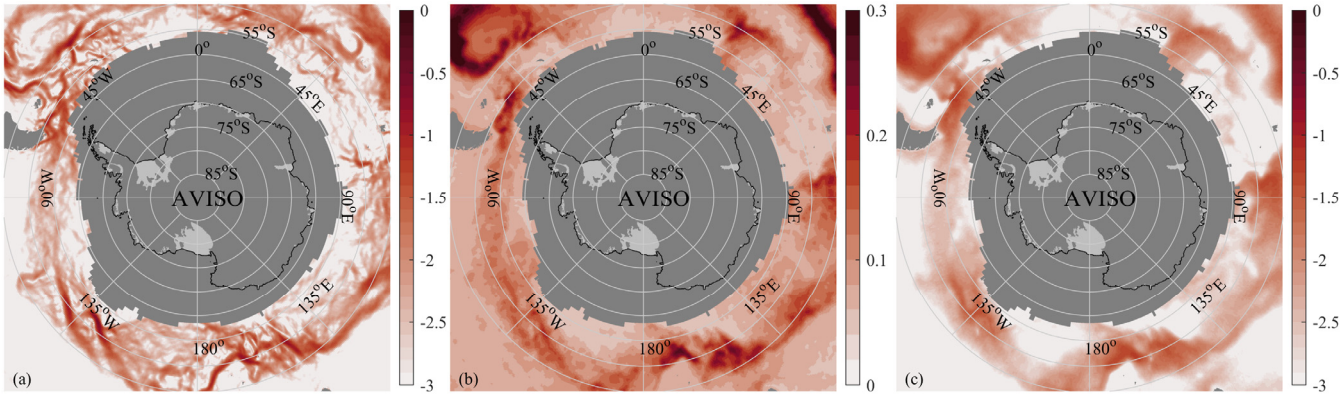

Fig. S11. The sea surface Kinetic Energy and the variability of η. **(a)** The $\log_{10}(MKE_{surf})$ (m^2 s^{-2}) in the AVISO. The grey region over the open ocean indicates the absence of year-round data in the AVISO. (b) and (a) As in (a), but for the STD of η (m) and the $\log_{10}(EKE_{surf})$ (m^2 s^{-2}), respectively.

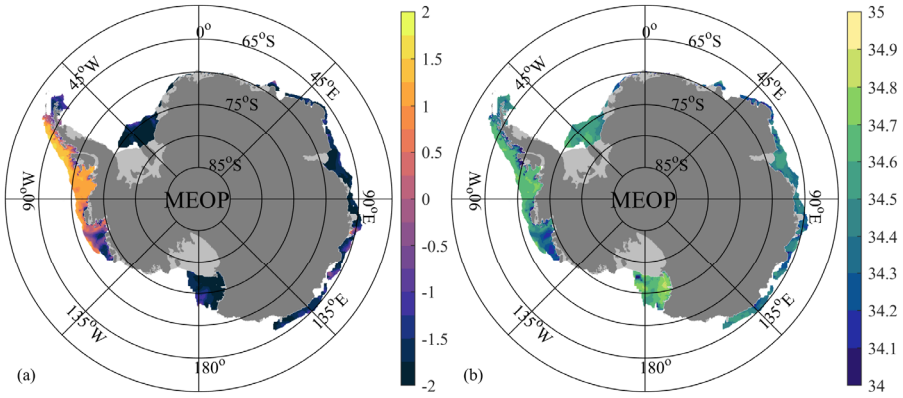

Fig. S12. The horizontal distribution of θ (°C) and S (psu) over the continental shelf. **(a)** Climatological θ at the bottom layer from the gridded MEOP. **(b)** As in **(a)**, but for bottom S.

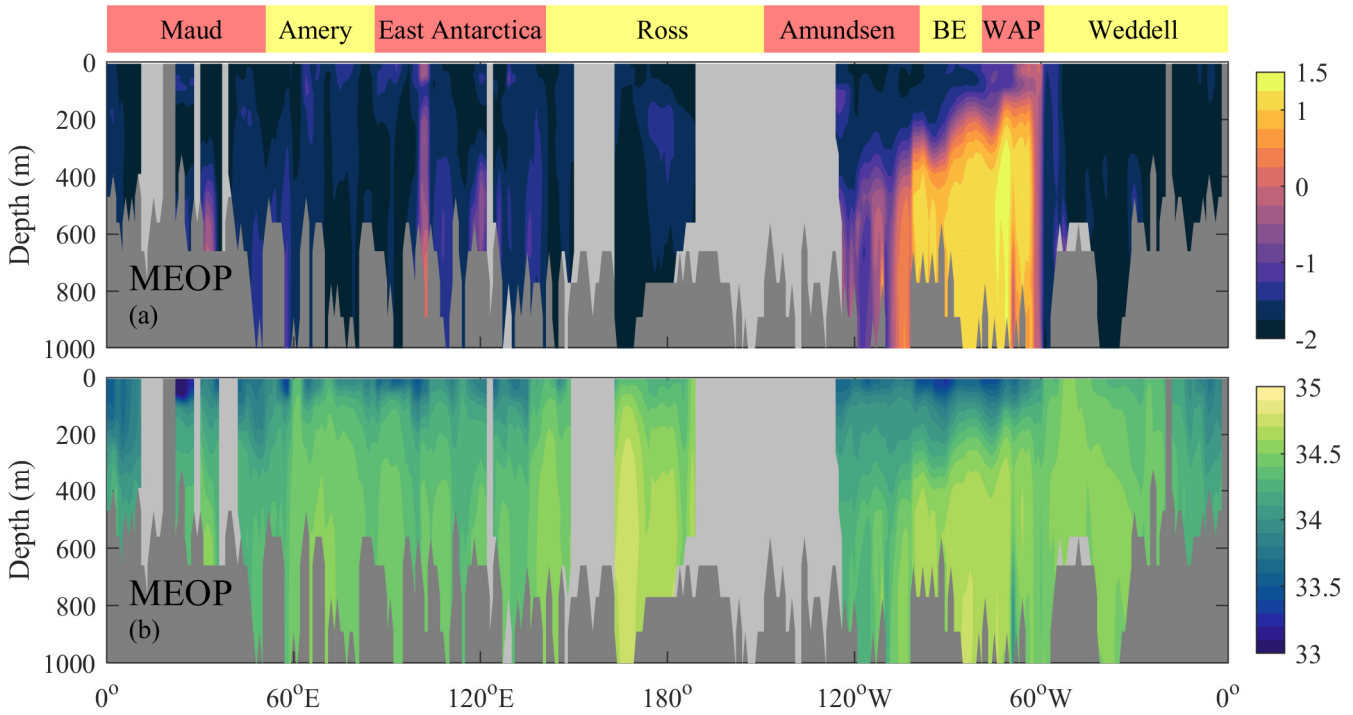

120 **Fig. S13.** The vertical structure of θ (°C) and S (psu) over the continental shelf. **(a)** Meridionally averaged θ over the continental shelf from the gridded MEOP. The light grey region indicates the absence of year-round data in the gridded MEOP. **(b)** As in **(a)**, but for S.

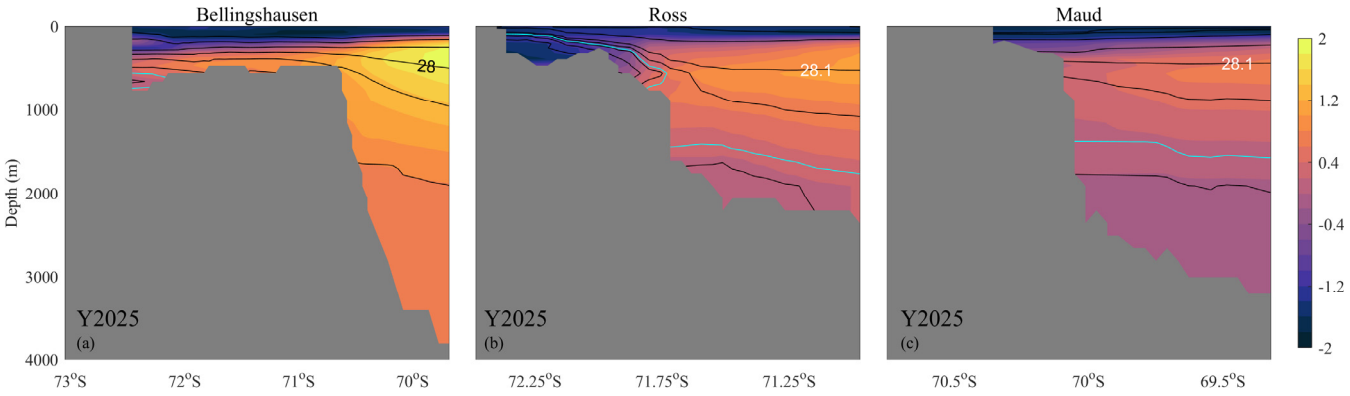

Fig. S14. The meridional structure of θ (°C) along the selected transects (blue lines in Fig. 5b) perpendicular to the continental slope. **(a)** Climatological θ along the selected transect in the Bellingshausen sector from Y2025. Black lines denote σ_0 (kg m^{-3}) in contour intervals of 0.1 kg m^{-3}. **(b)** and **(c)** As in **(a)**, but for the transects in the Ross and Maud sectors, respectively. The cyan lines denote the γ^n contour of 28.27 kg m^{-3}.

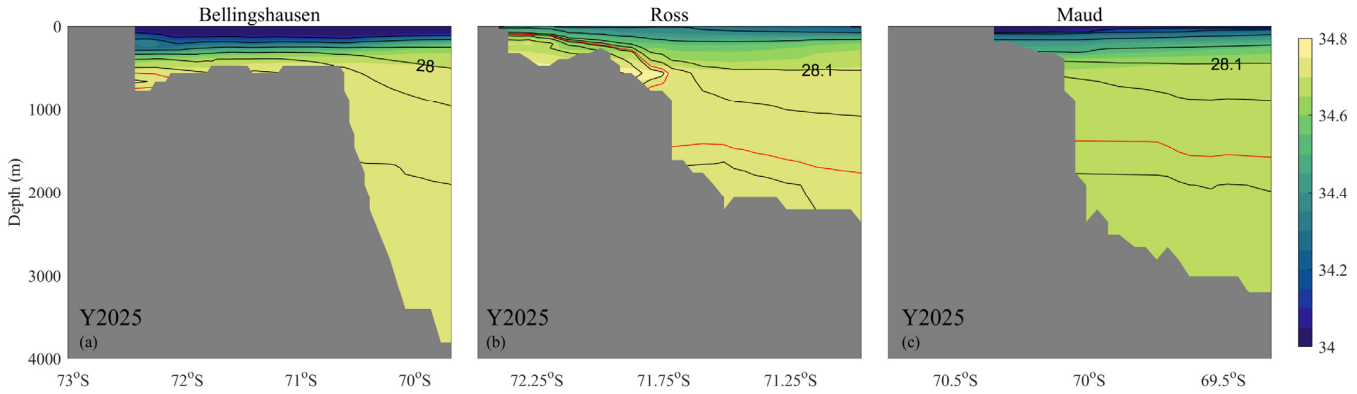

130 **Fig. S15.** As in Fig. S14, but for S (psu), with the red line denoting the γ^n contour of 28.27 kg m^{-3}.

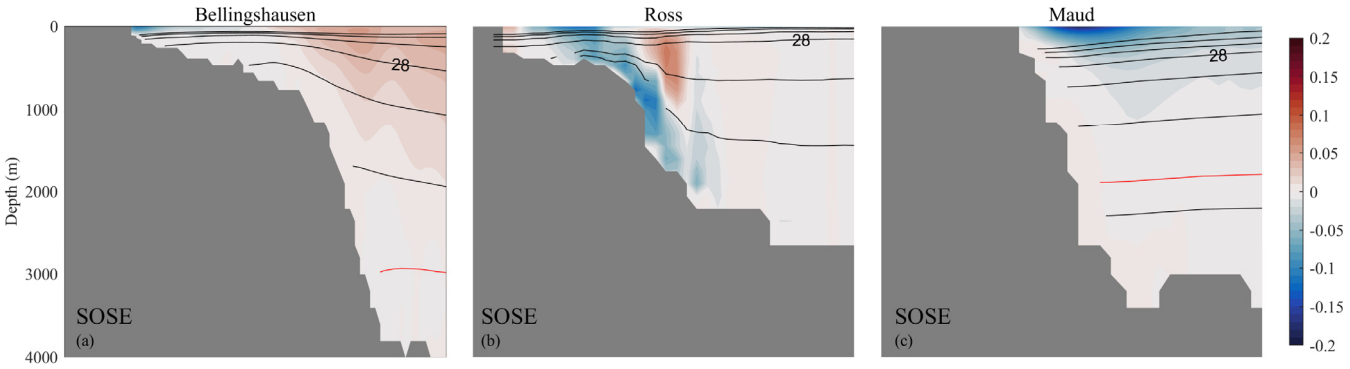

Fig. S16. The meridional structure of u_{along} (m s^{-1}) along the selected transects (blue lines in Fig. 5b) perpendicular to the continental slope. **(a)** Climatological u_{along} along the selected transect in the Bellingshausen sector from the SOSE. Positive values indicate a current flowing to the right of the down-slope direction (i.e., a generally eastward-flowing ASC). Black lines denote σ_0 (kg m^{-3}) in contour intervals of 0.1 kg m^{-3}. The red line denotes the γ^n contour of 28.27 kg m^{-3}. **(b)** and **(c)** As in **(a)**, but for the transects in the Ross and Maud sectors, respectively.

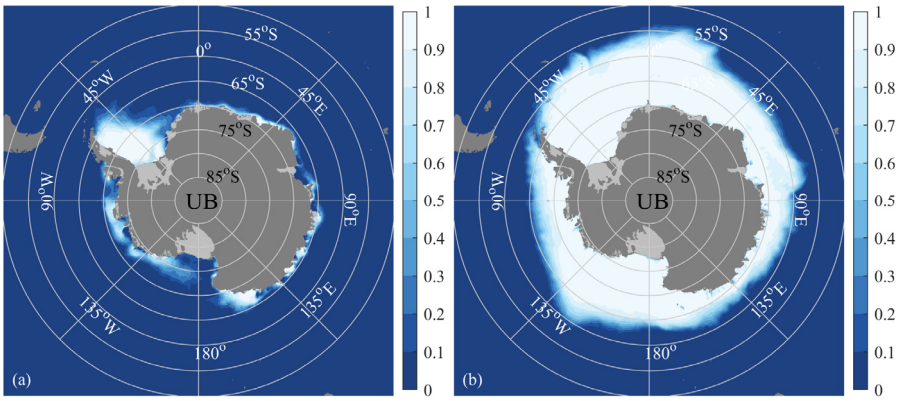

Fig. S17. The spatial pattern of SIC. **(a)** The satellite observed SIC in February from the UB. **(b)** As in **(a)**, but for September.

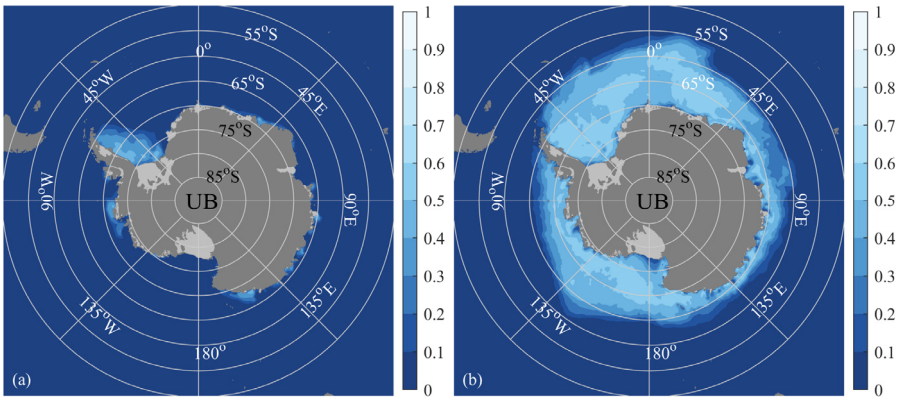

Fig. S18. As in Fig. S17, but for the SIT (m).

145

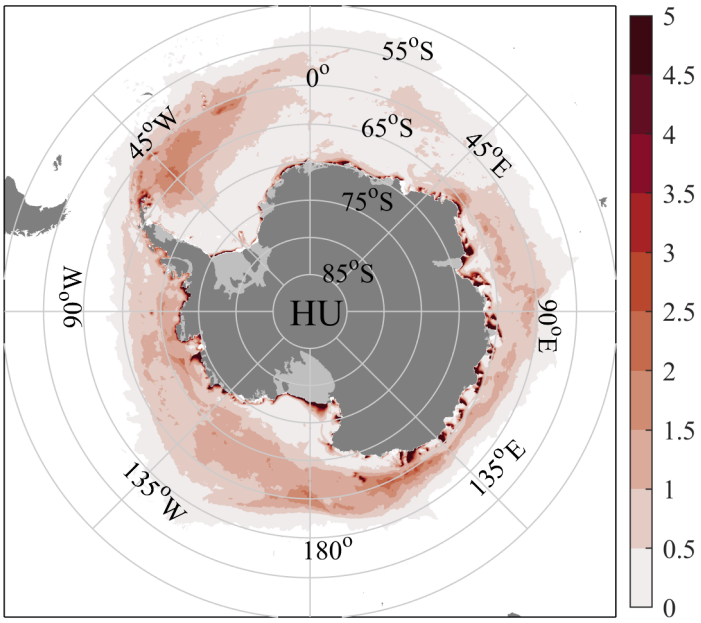

Fig. S19. The spatial pattern of estimated SIP (m yr^{-1}) during the freezing period (March-October) based on the AMSR-E by the HU.

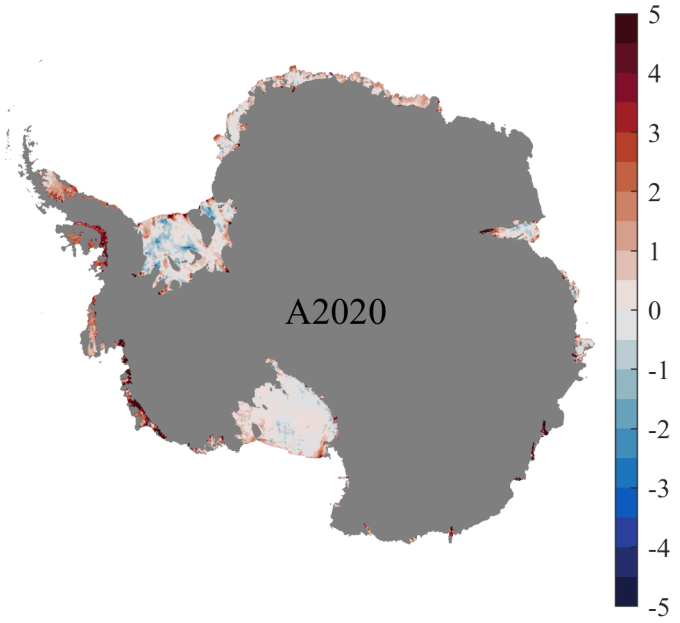

Fig. S20. The observed annual climatology of spatial pattern of SHI_{fw} (m yr^{-1}) from A2020.